Mirror Evaporator Improvement at SBU and Initial Coating Results

Preet Mann, Muqing Wang, Wenliang Li, Kong Tu

February 25, 2024

Abstract

This report presents improvements and design alterations made to the Evaporator System located in Stony Brook University Room S103, as well as an analysis of the techniques that are used, for general operation and the specific application of creating a mirror for pfRICH. The process of evaporation can be used to deposit a thin film of material upon a substrate, this requires a comprehensive vacuum system and a combination of metals to sublimate or evaporate. To adequately create the mirror, a procedure in which aluminum pellets are evaporated and chromium is sublimated resulting in a reflective finish is undergone, multiple modifications would be made to the interior of the existing setup of the evaporator as well as the exterior equipment to facilitate this. The process was modeled in ROOT and MATLAB, to provide a hypothetical deposition amount, and designs were created in Auto-desk Inventor, for ion-source frame set-ups. Throughout the process, numerous, multi-faceted, issues were to be addressed ranging from the required servicing of pumps to entirely new renderings of mounts and piping and leak testing. The processes of pumping down the system for vacuum, making changes to the water cooling, cryogenic pumping, and serialization of parts are documented within this work.

1 Introduction

1.1 Evaporation

Evaporation is a thin-film deposition technique, in which a metal is placed within a crucible, and then into a metal chamber. This system is pumped down to create a vacuum on the order of 10^{-8} atm, such that the system has no convection and the vapor can move freely. An electron gun then heats the metal to where it begins to evaporate or sublimate, from which the vapor travels and is deposited in an isotropic manner, as a function of the spectral power density and angle. This vapor would settle on a substrate and condense, ultimately forming the film layer, in the desired case a reflective coating. Physical vapor depositions require a vacuum, with evaporation most of all, which serves not only to provide an environment in which convection is not possible but also to increase the mean free path of the evaporated particles, such that they propagate straight until striking the surface. These atoms will either condense upon the surface to form a film or be re-evaporated, systems with fewer vacuums are prone to film contamination, requiring the use of high-grade vacuums and comprehensive pump-down processes to have adequate conditions.

1.2 Prior Work

The evaporator system, currently located at Stony Brook University room S103, had previously been constructed to create aluminum-coated petals, and as a result, was specifically engineered for that task. The system houses a set of large metal plates, connected by hinges to each other, that would support the substrate the film is being deposited upon. This framework would then be spun by a connected motor shown at the top of the evaporator to ensure the rate of deposition across the entire face of the substrate is consistent and to remove the time dependence for the amount of mass deposited after enough revolutions. The evaporator uses an e-gun to shoot a beam of electrons and melt the metals in the crucible, this e-gun is connected to a water chiller and a flow rate meter. Another connection is made for the turbo pump and roughing pump which serve to remove the initial gasses in the system. The entirety of the project was then set up with Veeco controllers and power supplies and placed

behind a bolted door with a mechanical gasket to prevent the introduction of dust, and moisture and help hold the vacuum. Many of these existing parts would be maintained and continued to be used for the pfRICH project.

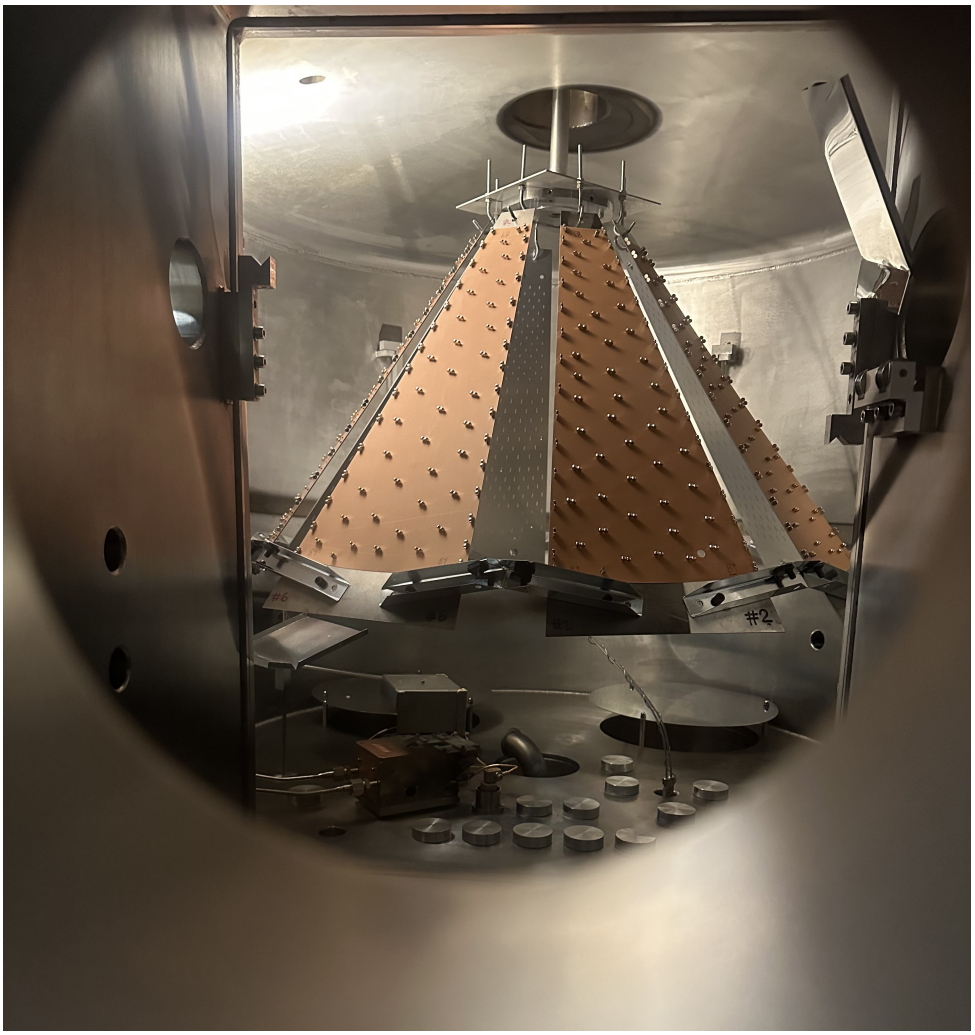

Figure 1: The image portrays the interior of the evaporator before any alterations

1.3 Evaporation for pfRICH

The improvements to the S103 evaporator were largely hardware changes to the system's water cooling, pumping, and mechanical fixtures. Note that the evaporator was never used for coating the reflective surfaces. Adding new mounting designs and introducing an ion gun served the purpose of having smoother and more uniform coatings for any given substrate, while new pipes were added to have better water flow to the electron gun. To create an adequate mirror for the proximity-focusing Ring Imaging Cherenkov detector (pfRICH), which is a critical component of the Particle-Identification system for the Electron-Ion Collider (EIC). To better understand and control the process, multiple calculations had to be done, specifically, how much mass would be deposited as the film upon the substrate in a given time frame, how long the evaporation should run, how much material should be deposited, if the substrate should rotate and for how long, as well as the appropriate mounting location so to receive an equal amount of coating at each location of the substrate. These calculations and answers would serve as a rough estimation and provide an expected value for the results of the evaporation process, from which we could work. The most crucial of which is the amount of mass deposited onto the surface as this determines whether the mirror could be created to the standard required and what steps could be taken to garner better reflectivity.

2 Modeling Mass Deposition

To begin coating, an adequate estimate for the rate of deposition, and the amount was to be determined. Deposition per area makes use of the system geometry, which is shown in Fig. 2, and is calculated via:

$$\frac{d\bar{M}_s}{dA_s} = \frac{\bar{M}_e cos(\theta) cos^n(\phi)(n+1)}{2\pi r^2} \tag{1}$$

in which the the deposited mass per unit area is equal to, the total evaporated mass $\bar{M}_e$, the cosine of the angle formed between the vector propagated from the source and the norm of the substrate $cos(\theta)$, the cosine of the angle between the source propagation vector and source normal raised to the averaged spectral power $cos^n(\phi)$, and the spectral power plus one $n+1$, all of which is divided by the area of the evaporator $2\pi r^2$. While ultimately an accurate representation of the mass deposition is acquired through these calculations, it neglects multiple aspects required for a true value, such as the change in spectral power as a function of crucible fill level and time elapsed. The rotational component resulting from the interior motor is another factor which despite being negligible after enough rotations, is not accounted for in this approximation as well as the substrate not located tangent to, or at the end of, the system. In practice, the mirror mounting frame and required angle for optimal deposition would be the determining factors in mirror placement, as well as the motor fixture needed to rotate the mirror for uniform deposition, if applicable.

In instances where the amount of mass in a crucible to be evaporated is unknown and or fixed deposition, such that the substrate is not rotated or moved for uniform deposition, it becomes pertinent to know the rate at which mass is lost from the source so to solve Eqn. 1. Multiple techniques can be applied to acquire this information, the first of which is simply by using a QCM or quartz crystal microbalance which reads the resonant frequency and resistance of thin films and near-surface-level depositions. As the frequency changes as a function of mass, the QCM would be able to be used to directly determine the amount of mass deposited per unit area at specific locations in a given cycle directly. Alternatively one could calculate mass evaporation and then apply it to Eqn. 1 via:

$$\bar{M}_e = \int_0^t \int_{A_e} \Gamma_e dA_e \, dt \tag{2}$$

where the total evaporated mass can be represented as the integral of the evaporation rate in mass units Γ_e concerning the surface area of the source and time. This value of evaporation rate is material specific but generally found via:

$$\Phi_e = \frac{\alpha_e N_A (P_v - P_h)}{\sqrt{2\pi MRT}} \tag{3}$$

$$\Phi_e = 3.513 \times 10^{22} \frac{P_v}{\sqrt{MT}} \tag{4}$$

Where Φ_e provides the evaporation flux, and at maximum flux where the coefficient of evaporation is $\alpha_e = 1$, and $P_h = 0$. The evaporation rate is then given by:

$$\Gamma_e = 5.84 \times 10^{-2} \sqrt{\frac{M}{T}} P_v \; [\frac{g}{cm^2 s}], \tag{5}$$

where M is the molar mass of the metal being heated, T is the temperature at which the metal is heated by the electron gun, and P_v is the vapor pressure in the chamber, which can be obtained via Eqn. 8 given the temperature to be known.

These formulas were used to define and write a code in ROOT that would provide a value for the mass deposition. For an approximation, the spectral power constant n was chosen to be 0.6. And since the substrate is in parallel with the power source in our evaporator system, the angles θ and ϕ are equal to each other. According to our measurement, the value θ at different locations of the evaporator is shown in Tab.1, and the surface area of the power source is $(6.413 \pm 0.713) \times 10^{-4} \; m^2$. Provided these constant values, including an estimated average evaporation rate $\Gamma \approx 10^{-4} \frac{g}{cm^2} sec^{-1}$, Eqn. 1 and Eqn. 5 are applied to find the estimated mass of Chromium and Aluminum deposited per unit area after 20-min evaporation, and the thickness of the coated layer can be easily obtained if we divide the surface mass density by the density of the metal. These results are shown in Tab.2. However, the

evaporation rate we used when estimating the deposition depth was later proven too small to be true after we compared the data acquired from the evaporation with our original estimations. This will be discussed in detail later.

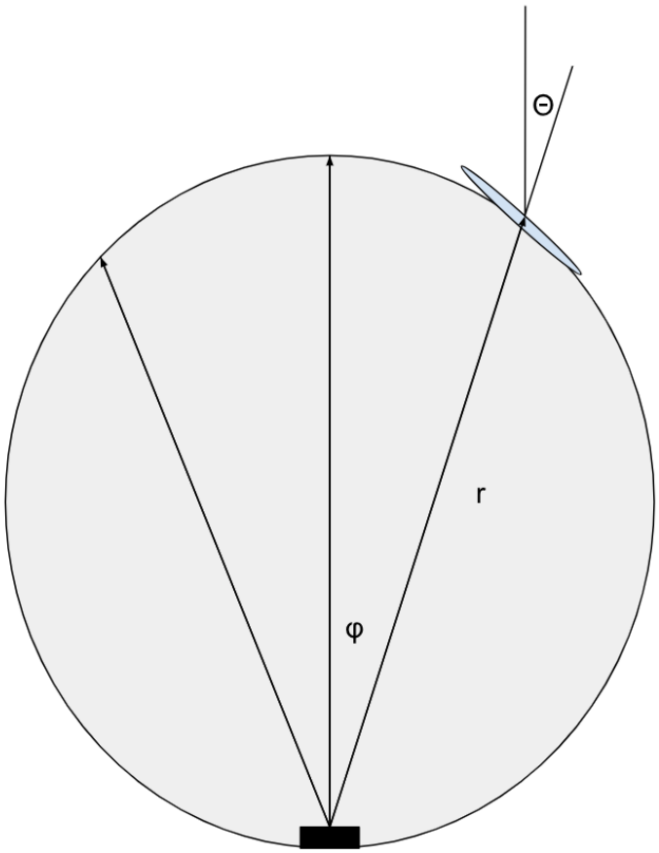

Figure 2: The image portrays the geometry behind mass deposition, with the dark box representing the emission source and the circle laying tangent to the main body being the substrate.

Location	θ (Rad)
Outer Corner	0.223 ± 0.010
Inner Corner	0.783 ± 0.026
Left Corner	0.546 ± 0.016
Right Corner	0.603 ± 0.015
Center	0.514 ± 0.015
Quartz depth monitor	0.627 ± 0.024

Table 1: Measured Angle θ at different locations in the Evaporator

Location	Estimated Depth of Cr Layer (kilo angstrom or kang)	Estimated Depth of Al Layer (kilo angstrom or kang)
Outer Corner	0.938 ± 0.107	2.471 ± 0.281
Inner Corner	0.349 ± 0.041	0.921 ± 0.108
Left Corner	0.661 ± 0.076	1.741 ± 0.200
Right Corner	0.494 ± 0.056	1.302 ± 0.149
Center	0.681 ± 0.078	1.794 ± 0.206
Quartz depth monitor	1.797 ± 0.211	4.733 ± 0.551

Table 2: Estimated deposition thickness of the Cr and Al layer in a 20-min evaporation period.

2.1 Spectral Power

The spectral power, given by the variable "n", is a quantity that changes with the fill level of the crucible and is subject to fluctuating with time. This value is not only difficult to find but not consistent, forcing the use of approximations. In ideal cases, it would be a value that results from the electron beam sweeping over the surface of the crucible, but as a result of the chromium pellets being uneven and rough in texture, it would mean the spectral power would be too variable to properly account for, especially as the surface changes as it's heated. The impact of this inconsistency is large on the estimation, for instance having 0 spectral means an entirely isotropic emission of particles from the crucibles and while the amount of material in the crucibles depletes, the spectral power value rises. This interaction ultimately results in non-uniform deposition despite constant current, vacuum, material, etc, and was identifiable in Fig. 12 (left), where the material in the crucible melted down the center, until the graphite layer of the crucible itself, and the rate of deposition spiked from 80 ang/s to 180 ang/s.

2.2 Skin and Penetration Depth

The skin depth and penetration depth are two parameters that help determine the amount of material deposition required. For instance, prior works chose the thickness of Al to be 20 times greater than the penetration depth of 233 nm light. The values for depth are attained from the following equations:

$$\delta_s = \sqrt{\frac{\rho}{\pi f_o \nu_\tau \nu_o}} \tag{6}$$

$$\delta_s = 2\delta_p \tag{7}$$

where ρ is the resistivity, f_o is the frequency, ν_τ represents relative permeability, and lastly ν_o is the permeability of free space. These constant values were then put into a ROOT program yielding a skin depth of 2.44266 nm and penetration depth of 1.22133 nm with an uncertainty of 0.01 nm. Most notably, the skin depth and penetration depth can be compared to the amount of material deposited to see the ratio of the thin film to the materials.

3 Preparation and Equipment Re-purposing

3.1 Water Chillers

The physical maintenance of the evaporator was largely to do with chillers that kept the turbo pump and electron gun cool. To have an adequate vacuum, a minimum of 10^-5 atm, the system would require a large pump down process, meaning two stable running chillers and pumps. The roughing pump is turned at the start and automatically engages the turbo pump after a specific threshold value, where the turbo will continue to run until the evaporation has concluded. As a result of this, the turbo pump is always in constant use and requires cooling. It is connected to a chiller at 55° F and slowly ramps up after being engaged, the longevity and stability of the turbo are crucial for any evaporation to occur at all, and as a result, the long-term maintenance of piping and chillers becomes a high priority. The system had two existing chillers, a Dynaflux R-2200V, connected to the turbo pump, and a Cornelius IMI Remcor CH750A connected to the e-gun. Of these two chillers, the Dynaflux chiller was largely unstable as it would not work for prolonged periods and eventually would

not work at all, whereas the Remcor chiller seemed stable for the time being. In attempts to repair the Dynaflux chiller, it was noted that the pump was seized and no longer moving water, with a new pump unavailable at the time, a temporary replacement chiller was found and substituted in for the first and second evaporations. Other smaller issues such as plastic tubing breaking down after wear also had to be addressed, a long-term solution was found by having spare chillers and motors due to the high uptime.

3.2 Cryogenic Pumping and Repairs

An immediate concern with the existing evaporator setup was an inability to reach necessary vacuums. While 10^{-5} atm to 10^{-6} atm is achievable, the mirror required a much lower value to produce the required results. This means cryo-pumping was going to be a necessary aspect of the pumping process for long-term results and one that had to be addressed. Cryopumps take advantage of the saturation vapor pressure of gasses, given by the Clausius-Clapeyron equation.

$$P_v \approx P_{initial} \cdot e^{\frac{\triangle H}{R} \cdot (\frac{1}{T_{initial}} - \frac{1}{T})} \tag{8}$$

where P_v is the vapor pressure, $P_{initial}$ is the initial pressure in the chamber, $\triangle H$ is the enthalpy of the vaporized material, R is the gas constant that is equal to $8.3145 J/(mol \cdot K)$, T is the temperature at which the metal was heated, and $T_{initial}$ is the initial temperature of the metal.

At specific temperatures, the gasses being pumped will condense, such that, the vapor pressure will be small enough to allow for the appropriate vacuum inside the chamber. As shown in the temperature vs saturation vapor pressure curves, Fig. 4 the cryopump will reach temperatures $\sim 17^\circ$ K to adequately reduce gasses such as CO, Ar, etc. into condensate. This cooling happens in two stages, an initial stage reaches $\sim 80^\circ$ K, and a second stage reaches $\sim 17^\circ$ K with a final charcoal layer to trap gasses such as He and Ne and slow their mean free path such that they do not return into the system. Here arose one of the first issues with cryopump for the existing evaporator, the original system used an Edwards Cryodrive 3.0, which was not functional. The cryohead required leak testing at all connections to see if it could be repaired, as well as not reaching adequate stage 2 temperatures, likely a result of the first issue. A detailed plan was then constructed on how to address the problems, the first idea of which was to acquire leak test fluid, apply it at joints, and visually test for bubbling. Secondly, a hand-held detector, ideally the Matheson 8067 which checks for the presence of gasses with a different thermal conductivity to air, was suggested to test the system while flushing it with UHP Helium. Ultimately a Varian Leak Detector system was found and despite needing to be serviced, it seemed like the most appropriate solution. After acquiring the needed helium, the system would be sprayed or filled and then connected to the intake valve and tested for the presence of a leak. Upon repairing the cryopump, there would be a large improvement to the quality of the vacuum and a subsequent decrease in several contaminants in the chamber, therefore creating a more even and uniform reflective coating.

Figure 3: The image shows the existing Varian Leak Detector, despite requiring repairs and servicing it appeared to be a likely candidate to use for testing the connections.

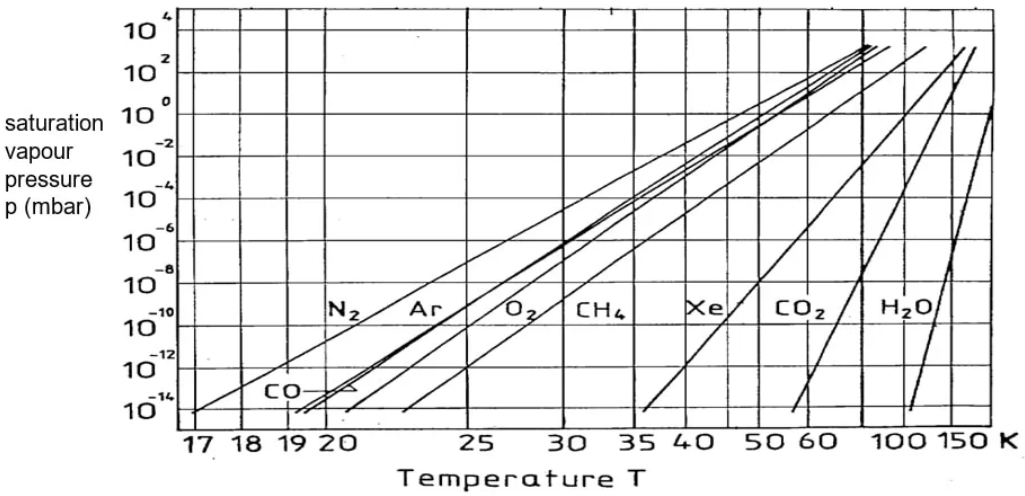

Figure 4: Depiction of the vapor saturation curve for multiple gasses

3.3 Mounting

The existing lampshade fixture was much too large and therefore not an appropriate manner of mounting the small samples that we planned to coat, as a result, it was disassembled and a new mounting scheme was planned. The lampshade (shown in Fig. 1) used magnets to hold large aluminum petals against its body, and would then be hooked onto a motor arm to provide the rotation for smooth coating. This would provide the template for our design, keeping the top base plate and manufacturing a new fixture to which the samples could be either clamped or attached via adhesive and left to spin safely in the chamber. After developing a CAD model of the fixture, we proceeded to take

Figure 5: Shows the new mounting scheme, at the bottom of which samples would be taped or clamped onto.

an aluminum sheet and drill holes where metal rods could be inserted and connected to the initial plate. This entire body was then inserted into the chamber and threaded around the motor arm to be spun on the order of 1 revolution per second in both clockwise and counterclockwise rotation to ensure stability. Ultimately VHB adhesive was used on the back of samples to attach them onto the new metal plate to hold them throughout the length of the evaporation, this tape was tested in an initial pump down to test whether the possibility of out-gassing was a concern. The true mirror for the pfRICH project would be much larger than 2-inch samples and would therefore require an entirely new mounting scheme, separate from the one devised for the smaller test evaporations.

4 Evaporation

In this report, we provide details of two independent evaporation attempts: the 1st evaporation was carried out on Nov.17th, 2023, and the 2nd evaporation was on Nov 30th, 2023. See their information in the paragraphs below.

4.1 First Evaporation

Detailed recordings of prior evaporations, done by the TPC group, served as the backbone for the first run, from which the amount of material deposited and the methodology for the procedure were created. The mounting fixture with Lexan 8010 (10 mil thickness) [1] and CMA samples adhered by tape was connected to the motor inside of the chamber. Two crucibles were then selected and measured, at 5.06 grams and 5.1 grams each, to which aluminum and chromium would be added and then placed in the chamber. Proper guidelines were created to determine the bounds for evaporating, where 20 kang or 20 minutes were found to be the threshold for chromium and 30 kang or 20 minutes was the threshold for aluminum. After establishing proper water flow to both the e-gun and pumps of the chamber and

[1] Lexan 8010 polycarbonate film at 10 mil thickness: https://www.tekra.com/products/films/polycarbonate-films

the components were checked over, we could begin pumping down for evaporation. The chamber was then left to pump for two days to ensure the lowest possible vacuum.

Process

The evaporation procedure begins by starting the pump down and roughing the pump, this allows for the chamber to come down to $\approx 3\times10^{-3}$ torr from which the turbo pump automatically engages. After then reaching 10^{-6} torr, the e-gun is powered on to 6.6 kV, and the appropriate raster pattern is chosen for the base chromium coating. With the shutter covering the crucible, the intensity of the current is slowly increased until the desired amount is reached. In practice, this process was done too slowly, after removing the shutter the chromium immediately began to deposit at 100 ang/second, reaching 40 Kang in 13 minutes. The current is then ramped back down and the crucible and raster patterns are switched to those corresponding to aluminum. The procedure is then repeated by covering the crucible, ramping up the current, and then allowing the shutter to move out of place to have deposition occur. The aluminum formed a much thinner layer, at a peak of 25 angstroms/second and a total of 20 kang, as a result of less current despite more time (30 min).

Outcome

Multiple samples developed a coating, most of which were not reflective and unable to produce a clear image. This is likely a result of thick chromium deposition and not enough aluminum. Two samples, namely the 1/4 CMA, were able to develop reflective and relatively uniform coatings, but suffered from systematic imperfections, specifically a small circle in the center of the samples where it is suspected they were cut and a fingerprint. These issues with unclean samples would hinder the reflectivity and would provide areas for improvement. It was also noted the Lexan samples were unable to develop an adequate coating as they had a protective plastic layer on top of their surface that had not been removed. Multiple strategies for improvement were developed, primarily having thinner chromium deposits and introducing a second crucible of aluminum, allowing for more deposition. The initial run used crucibles of 5.06 g and 5.10 g for chromium and aluminum and was then filled with 7.12 g and 3.65 g respectively. Of the 3.65 g of aluminum, the evaporation only expended 0.54 g meaning that subsequent evaporations would need to run for more time and at higher currents.

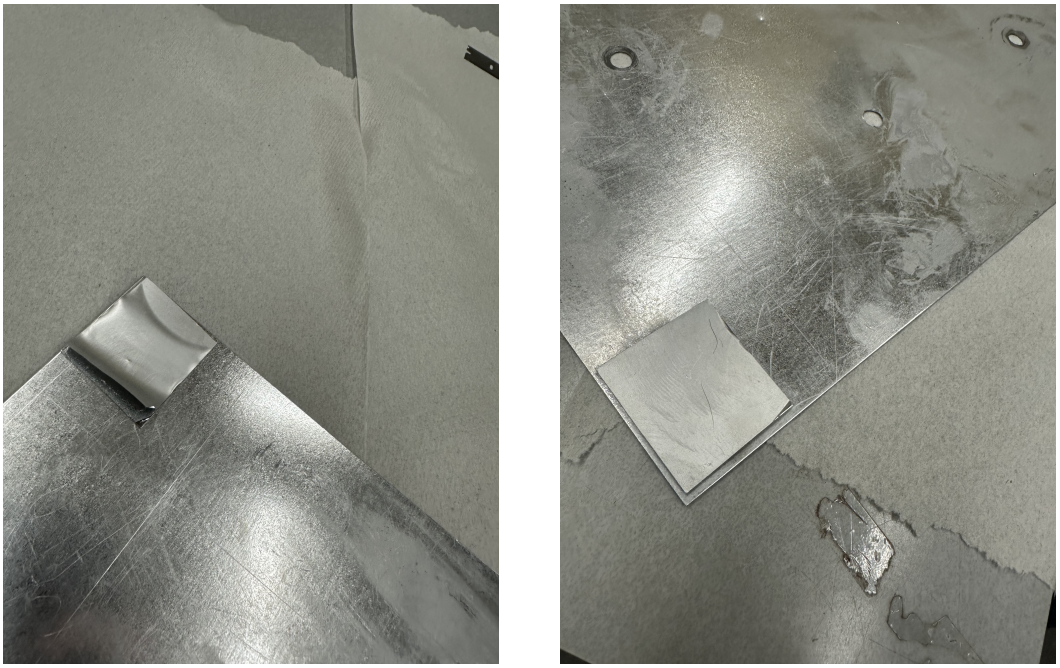

Figure 6: Left: shows Lexan Sample with the protective film not removed, as a result, the coating peels off. Right: The Lexan sample developed a dull coating onto the protective film, the corner appeared reflective as the film had come off and the Lexan was directly coated.

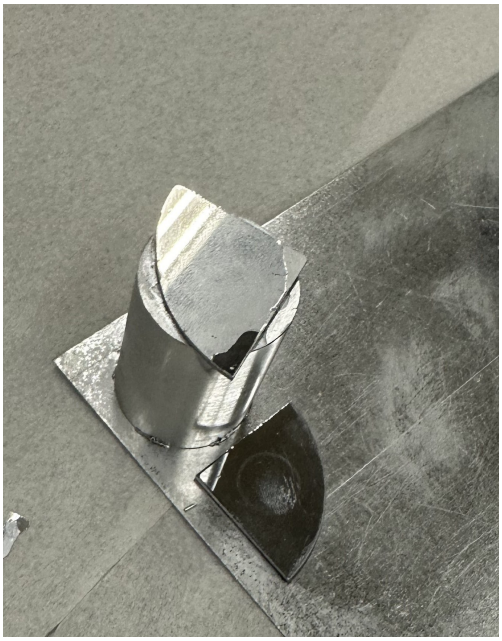

Figure 7: Two 1/4 inch CMA samples, the one shown on a post were likely contaminated and developed a poor coating while the lower sample appears reflective, the systematic circle from the cutting of the pieces is shown as well as a fingerprint from prior mishandling.

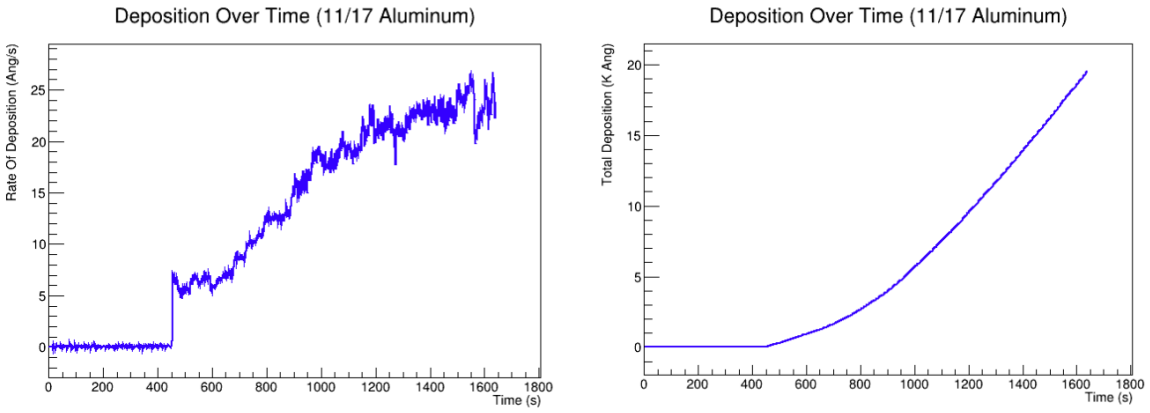

Figure 8: Aluminum deposition rates (left) and accumulated deposition (right) graphs as a function of time.

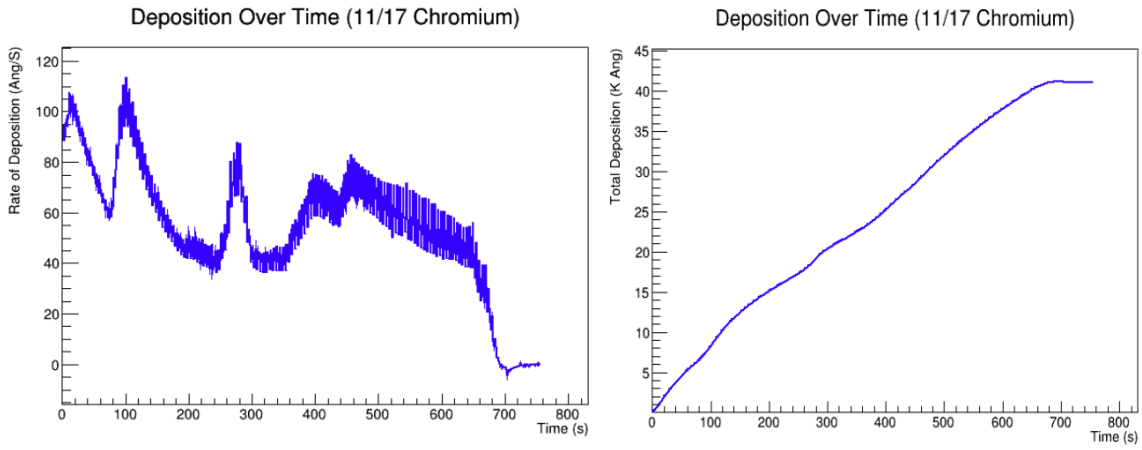

Figure 9: Chromium deposition rates (left) and accumulated deposition (right) graphs as a function of time, as the start of this data was collected as the evaporation had already begun, hence a non-zero starting value for the rate of deposition

4.2 Second Evaporation

The second evaporation aimed to apply the lessons we learned from the first, primarily to remove the protective film on the Lexan samples to adequately coat them and to have increased aluminum deposition time. Reducing chromium deposition was another key aspect of the second evaporation, meaning less time was spent on the chromium crucible and at a lower current whereas each aluminum crucible saw larger currents, leading to a 5 times larger rate of deposition.

Process

The samples were mounted using the same technique, VHB acrylic adhesive onto the metal fixtures, this time including multiple carbon fiber samples, full 2-inch CMA samples, and 2 Lexan samples. The aluminum crucibles were increased from 3.5 g to 5 g each and the chromium was kept at the same 7 g, all 3 were then inserted into the carousel of the e-gun. The techniques stayed relatively the same, with the ramp-up on the chromium being slightly faster than the initial run and making sure aluminum reached 30 kang for each crucible.

Outcome

The second evaporation resulted in more consistent coatings across different samples, with the CMA samples and Lexan, being the most successful, having clean and undisturbed coatings but the carbon fiber being dull and unreflective due to the large cuts and rough surface of the raw material. Notably during the evaporation, too much time was spent on the aluminum crucibles, resulting in the centers being almost entirely evaporated away and uneven rate of deposition shown in Fig. 11 and Fig. 12 (left). Ultimately a total of ≈ 75 kang of aluminum was deposited and 15 kang of chromium during the evaporation, creating seemingly more reflective coatings. The relative and absolute reflectivity of these mirrors was to be tested at 40° with the next steps being a cleaning procedure for the substrate, by ultrasonic bath, as well as further reducing the amount of chromium and conducting a thickness test (see 1/4 CMA sample with grid pattern Fig. 12) to determine the amount of deposition from the chromium and aluminum, as all prior values were only amount deposited on the QCM and a ratio to convert them had to be applied. This thickness value would provide further value in corroborating any deposition predictions that were modeled as well as giving an indication of how much time, current, and material amount relates to film deposition in a practical application. According to the measurement carried out by Bent Nelson, the total depth of the coated layer on a mirror shown in Fig. 13 after these two evaporations is 1.3 μm.

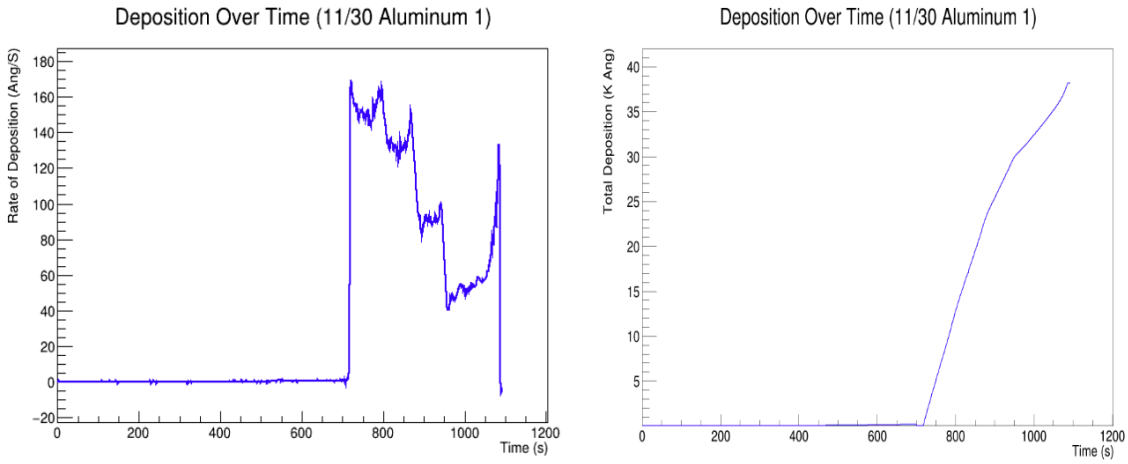

Figure 10: The deposition rate and amount, over the 20-min time interval for the first aluminum crucible

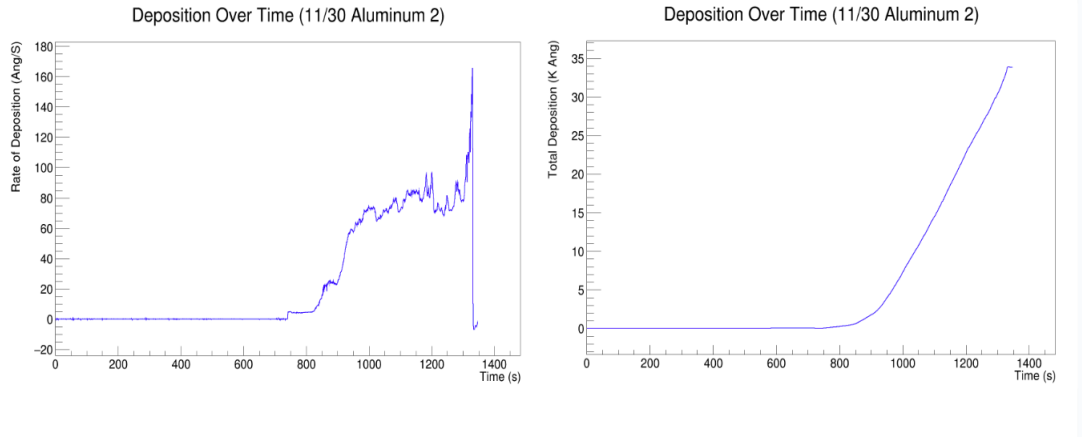

Figure 11: The deposition rate and amount, over the 25-min time interval for the second aluminum crucible

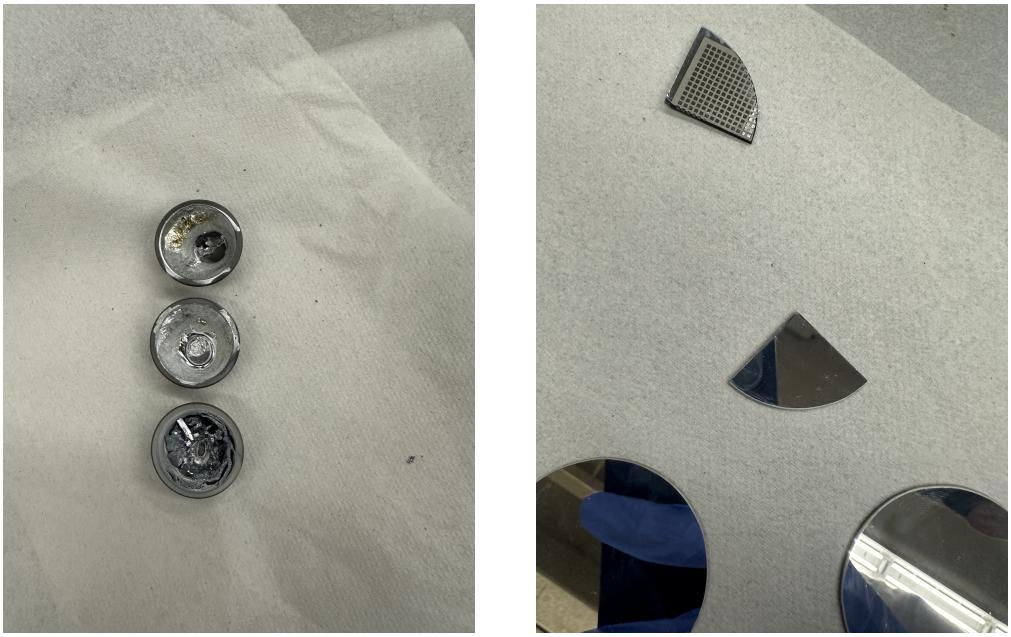

Figure 12: Left: Shows the chromium and aluminum crucibles, with chromium being the bottom-most, where it is notable that the aluminum crucibles have lost a large amount of material from the center and the graphite bottom is becoming visible. Right: Results of the second evaporation test, the topmost 1/4 CMA sample serves the purpose of thickness testing.

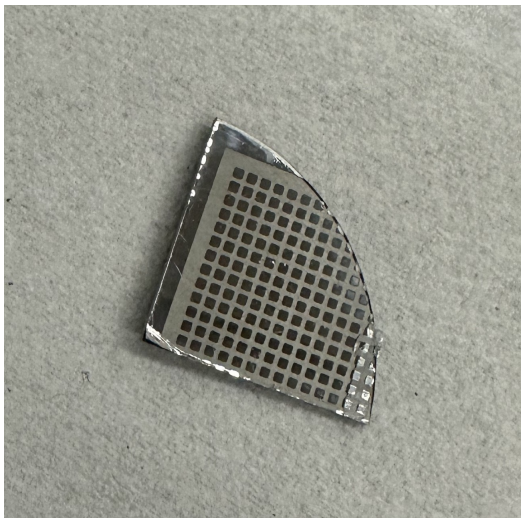

Figure 13: The mirror piece (control sample for thickness) on which the depth of the coated layer was measured. The area on which the grid covered during the evaporation wasn't coated, and other areas have a coated layer.

4.3 Reflectivity measurement

The criteria of the pfRICH mirrors were stated to be 90% reflectivity in the low UV to the visible spectrum of light, the guide for which would be relative and absolute reflectivity tests on the samples created in the test evaporations. A setup involving a beam striking an initial reference mirror, of known reflectivity, then hitting the test mirror and subsequently entering an integrating sphere from which the beam exists, allows for a reflectivity measurement of the test mirror, the one before the integrating sphere. This can be adjusted to any angle, specifically for the 45° relevant to this project and an appropriate value for the smaller mirrors can be determined. The absolute reflectivity measurements

were done relative to a known 100% reflectivity mirror, such that the light reflected off the first mirror will be the entirety of the incident light and any losses will be a direct result from the experimental mirror. Multiple reflectivity trials were conducted for all the samples, with the carbon fiber providing the weakest results with it being at best 65% reflective, occurring at 300 nm, and worst 36% reflective at 390 nm. The Lexan fared slightly better, with a peak of 82% at 480 nm and a low of 63% at 360 nm, generally around 70%. The 2-inch CMA samples seemed to be the most reflective, averaging an absolute reflectivity nearing 75% with a peak at 83% at 500 nm and a low at 67% at 330 nm. Moving forward multiple steps can be taken to improve these values, namely a proper cleaning procedure in the form of an ultrasonic bath and using lens paper in the handling or transport of samples would be highly beneficial, as well as further decreasing the chromium deposition to create a less thick and ideally more uniform coating.

Figure 14: Depicts the reflectivity of the first set of samples, ranging from 300-500 nm wavelength ± 2 nm

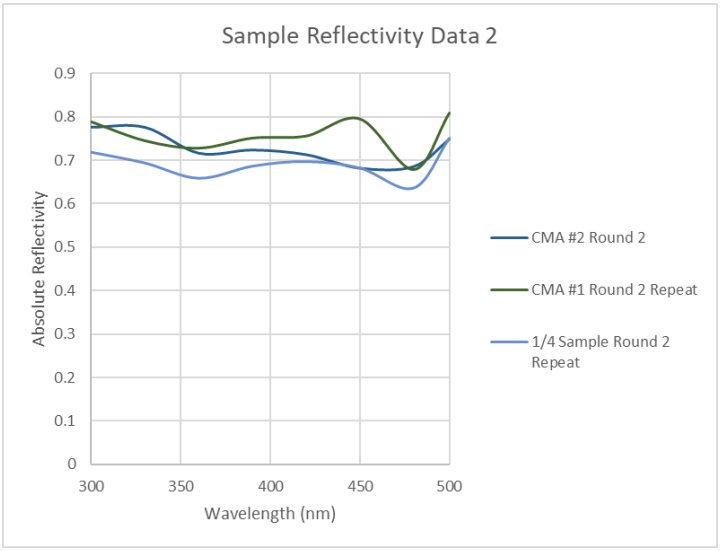

Figure 15: Portrays the reflectivity of the second set of samples, ranging from 300-500 nm wavelength ± 2 nm

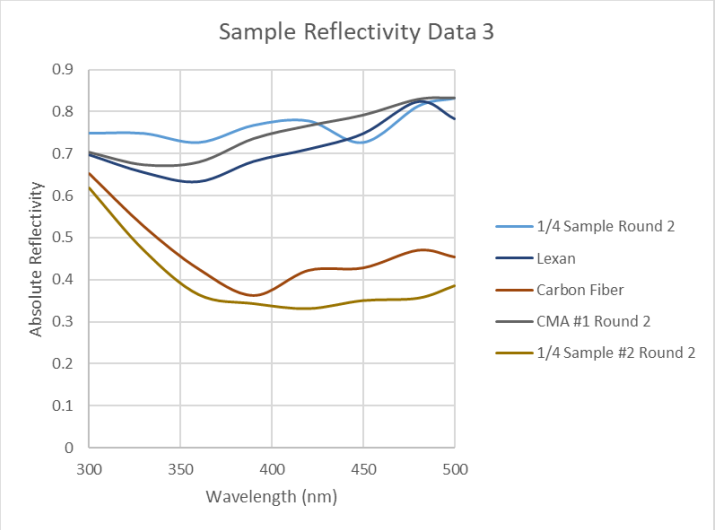

Figure 16: Portrays the reflectivity of the third set of samples, ranging from 300-500 nm wavelength $\pm$ 2 nm.

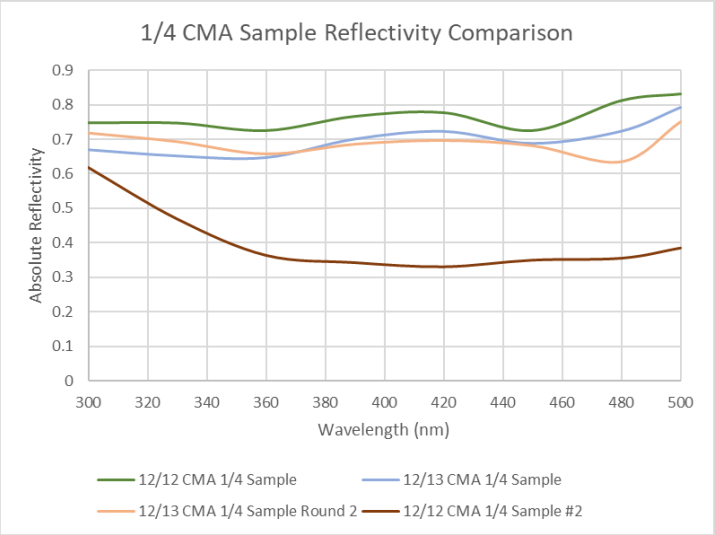

Figure 17: Comparison of all quarter CMA reflectivity trials, across two days.

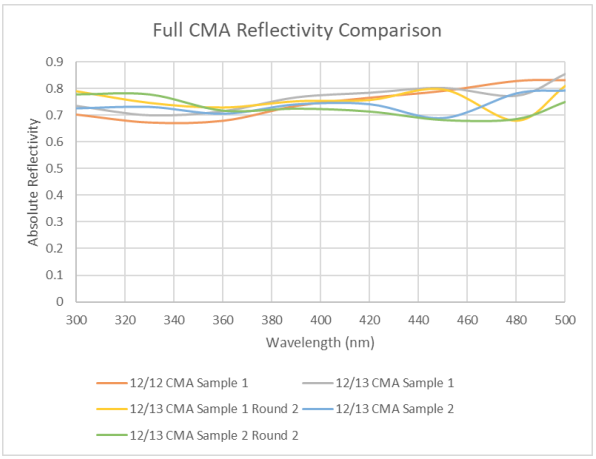

Figure 18: Compares the reflectivity of full 2-inch CMA samples across multiple trials.

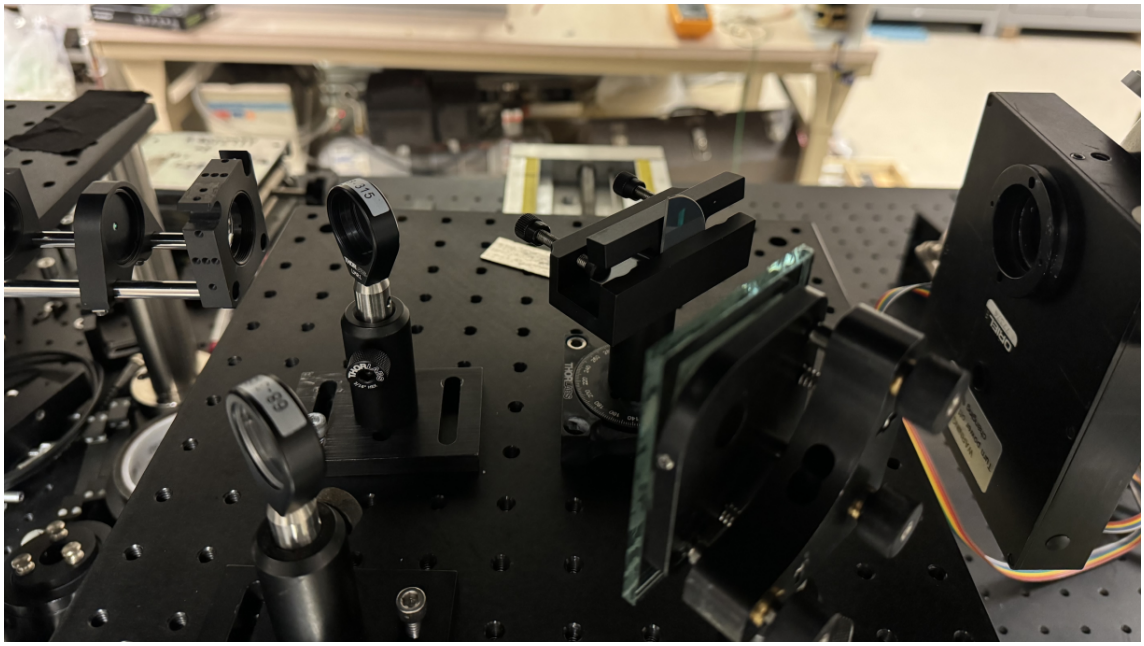

Figure 19: Shows the mechanical setup for the reflectivity measurement, where a known mirror is placed followed by a test mirror.

12/13/2023

	CMA #2 Round 2		EIC 6J		CMA #1 Round 2 Repeat		1/4 Sample Round 2 Repeat		EIC 1J Repeat	
Wavelength (nA) +- 2 nm	Relative	Absolute	Relative	Absolute	Relative	Absolute	Relative	Absolute	Relative	Absolute
300	0.85	0.7246794872	1.00	0.85	0.87	0.7355769231	0.79	0.6701923077	0.93	0.7927884615
330	0.81	0.730239521	1.00	0.9	0.78	0.7005988024	0.72	0.6520958084	0.94	0.8461077844
360	0.78	0.7046590909	1.00	0.9	0.80	0.7159090909	0.72	0.6473863636	0.98	0.8846590909
390	0.82	0.7398773006	1.00	0.9	0.85	0.7674846626	0.78	0.7012269939	1.02	0.9193251534
420	0.82	0.7403773585	1.00	0.9	0.87	0.7845283019	0.80	0.7233962264	1.04	0.9339622642
450	0.76	0.6884792627	1.00	0.9	0.89	0.8025345622	0.76	0.6884792627	1.01	0.9082949309
480	0.87	0.7808823529	1.00	0.9	0.86	0.7733193277	0.80	0.7241596639	1.14	1.024789916
500	0.88	0.7915254237	1.00	0.9	0.95	0.8542372881	0.88	0.793220339	1.06	0.9508474576

	CMA #2 Round 2		EIC 6J		CMA #1 Round 2 Repeat		1/4 Sample Round 2 Repeat		EIC 1J Repeat	
Wavelength (nA) +- 2 nm	Relative	Absolute	Relative	Absolute	Relative	Absolute	Relative	Absolute	Relative	Absolute
300	0.91	0.776975945	1.07	0.9113402062	0.93	0.7886597938	0.85	0.718556701	1.00	0.85
330	0.86	0.7767515924	1.06	0.9573248408	0.83	0.7452229299	0.77	0.6936305732	1.00	0.9
360	0.80	0.7168786127	1.02	0.9156069364	0.81	0.7283236994	0.73	0.6586127168	1.00	0.9
390	0.80	0.7243243243	0.98	0.8810810811	0.83	0.7513513514	0.76	0.6864864865	1.00	0.9
420	0.79	0.7134545455	0.96	0.8672727273	0.84	0.756	0.77	0.6970909091	1.00	0.9
450	0.76	0.6821917808	0.99	0.8917808219	0.88	0.7952054795	0.76	0.6821917808	1.00	0.9
480	0.76	0.6857933579	0.88	0.7904059041	0.75	0.6791512915	0.71	0.6359778598	1.00	0.9
500	0.83	0.749197861	0.95	0.8518716578	0.90	0.8085561497	0.83	0.750802139	1.00	0.9

Figure 20: Displays the relative and absolute reflectivity of 1/4 CMA, Lexan, carbon fiber and 2 inch CMA.

4.4 Comparing Measured Deposition Depth to the Calculations

When we looked back on our previous estimation of the coated layer depth (using the methodology described in Sec. 2), we found a discrepancy of about a factor of 10, as is shown in Tab. 3. Given this issue, we double-checked the estimation process and found out that we may owe the discrepancy mostly to the unreasonably small ideal evaporation rate that we took before, which is $\Gamma \approx 10^{-4} \frac{g}{cm^2} s^{-1}$. If this is a reasonable value, then after the 20 min evaporation only 1.2 g of Al will be evaporated, which is far smaller than the actual evaporated mass.

Evaporated Metal	Time (min)	Deposition Depth on Quartz (kang)	Initially Estimated Depth (kang)
Cr (1st)	11.472	41.108	1.031
Al (1st)	19.798	19.526	4.621
Total (1st)		60.634	5.652
Cr (2nd)	8.000	16.127	0.719
Al (2nd, round 1)	6.192	38.169	1.465
Al (2nd, round 2)	8.791	33.808	2.080
Total (2nd)		88.104	4.264

Table 3: Discrepancy between the measured and initially estimated deposition depth on the quartz monitor. Here, 1st and 2nd are referring to the two coating attempts summarized in Sec. 4.1 and 4.2.

Evaporated Metal	Time (min)	Deposition Depth on Mirror (kang)	Initially Estimated Depth (kang)
Cr (1st)	11.472	6.066	0.391
Al (1st)	19.798	2.881	1.751
Total (1st)		8.947	2.142
Cr (2nd)	8.000	2.380	0.273
Al (2nd, round 1)	6.192	5.632	0.555
Al (2nd, round 2)	8.791	4.988	0.788
Total (2nd)		13.000	1.616

Table 4: Total evaporation time, actual deposition thickness, and estimated deposition depth for the 1st and 2nd coating. Note that there are two rounds of Al coating. Here, 1st and 2nd are referring to the two coating attempts summarized in Sec. 4.1 and 4.2.

Tab. 4 demonstrates the discrepancy between the measured and initially estimated deposition depth

on the mirrors. Note that in the actual coated deposition thickness column, only the total depth after the 2nd evaporation was precision measured which is 1.3 micrometers (or kang), the control sample used for determining the thickness is shown in Fig. 13. This measurement was performed by Bent Nielsen [2]. All other thickness numbers were extrapolated through the known ratio between the total depth on the depth measured and on the quartz monitor, and the ratio of coated depth between different rounds of evaporation.

After carrying out those two evaporations, we found it necessary to find a way to manipulate the evaporation rate Γ_e via changing the applied heating current I, to tune the coated depth in our future trials. To figure out the relationship between Γ_e and the current, other than the equation for evaporation rate (Eqn 5) and the Clausius-Clapeyron Equation (Eqn. 8), we also need the relationship between the change of temperature $\triangle T$ of the metal during the i-th second of evaporation and the applied heating current I, which is:

$$(\triangle T)_i = \frac{(E_{absorbed})_i}{m_i \cdot c} = \frac{IV\triangle t}{m_i \cdot c} = \frac{IV\triangle t}{[m_{i-1} - A \cdot (i-0.5) \cdot \triangle t \cdot (\Gamma_e)_i] \cdot c} \tag{9}$$

where V is the applied voltage, which is constant in the evaporation, $\triangle t$ is 1 second, m_i is the left-over mass of the metal being heated during the i-th second, c is the specific heat capacity of the metal, m_0 is the mass of the metal at the beginning, and A is the area of the power source, which is $(6.413 \pm 0.713) \times 10^{-4}\ m^2$ according to our measurement.

Using Eqn. 5, Eqn. 8, and Eqn. 9, we derived the following formula for the evaporation rate Γ_e at the i-th second of the evaporation:

$$(\Gamma_e)_i = 0.584 \cdot P_{i-1} \cdot \sqrt{\frac{M}{T_i}} \cdot exp\ [\frac{\triangle H}{R}(\frac{1}{T_{i-1}} - \frac{1}{T_i})] \tag{10}$$

where

$$T_i = T_{i-1} + \triangle T_i \tag{11}$$

In the above formula, P_i and T_i are the pressure and temperature at the beginning of the i-th second, and P_0 and T_0 are the known initial pressure in the chamber and the initial temperature of the metal being heated.

But there is a difficulty that remains unsolved so far. The equation we got is an implicit one with Γ_e on both sides. We have tried to put Γ_e on one side of it using different computational methods, but haven't succeeded yet. In the coming future, we will keep trying to modify Eqn.10 and Eqn. 11 to express Γ_e as a simple function of the applied heating current I and the voltage V. We will testify to our assumption by comparing the outcome with the data we got, and keep modifying our assumption accordingly.

5 Conclusion and Future Remarks

Mirror coating development at SBU has seen much progress and a long-term plan was developed for further improvements. In terms of the preparation and handling, the first new coating attempts suggested the following lessons:

- A more adequate cleaning of the substrate surfaces: note that due to surface contaminates induced during the sample cutting process, a stronger solvent and ultrasonic bath are recommended.
- Creating appropriate mounting mechanisms for the mirror substrate: minimizing the duration and complexity during the mounting procedure.
- Building spare part inventory and equipment maintenance: involving chillers, pumps, etc are paramount to the project.

The findings from the first few coating attempts could be summarised as the following:

[2]Bent Nielsen: Senior Lab Instruction, Department of Physics, Stony Brook University. bent.nielsen@stonybrook.edu.

1. The initial measurement of 75% reflectivity at 300 nA measured at 40° reflection angle with the best coating quality CMA samples with ISO N1 smoothness (corresponds to the smoothness of 25 nm) appears to be the most promising.

2. The direct coating onto the carbon fiber substrate yields 20-30% less reflective. Furthermore, the localized irregular deep scarf mark will further degrade the reflectivity.

3. Lexan samples gave comparable results to the CMA samples which open the possibility of using it as a coating material, after bonding it to the carbon fiber substrate.

4. From the 1st evaporation, the deposited Cr thickness is 6.07 kang, and the Al layer thickness is 2.88 kang. From the 2nd evaporation, the deposited Cr thickness is 2.38 kang, and the Al layer is 10.62 kang.

5. A Thinner layer of Cr and a thicker Al layer seem to be the formula for improving the reflectivity. The optimal layer thickness requires further investigation.

Besides the conclusive remarks, a few future upgrades are critical for improving the reflectivity quality:

1. Installing the ionized gun: this could improve the localized smoothness as the deposition material accumulates on top of the coated substrate.

2. Restring the cryo-pump vacuum system: improving the vacuum capability from 10^{-6} to 10^{-9} torr.

Another important objective is to better understand the coating capability and evaporation rate of the current configuration. This can be achieved by comparing the mathematical prediction to the coated layer's thickness based on live monitoring and measured deposited thickness on controlled samples. With the actual deposited depth on the Quartz and the total depth on the second round of evaporation to be known, we got the actual deposited depth on the mirrors in each round of evaporation via calculation and found a discrepancy by a factor of 10 to 20. Based on the results from the first few coating attempts, we optimized a few critical parameters to fine-tune our evaporation/deposition rate estimation capability. In the subsequent trials, we will further inspect and adjust the evaporation rate Γ_e by altering the applied heating current and voltage to tune the depth of the coated layer. We hope to perfect the algorithm to be able to predict the deposition depth to the factor of 2 to the measurement currently, the prediction is accurate within 1 order of magnitude.

Acknowlegement

We would like to express our special gratitude to Rudy Begay, Thomas Hemmick, Ross Corliss, and Vassu Doomra, for their suggestions, expert opinions, and knowledge. Special thanks to Bent Nelsen, Andreas Jung, and Sushrut Karmarkar for providing critical measurements cited in this report. We also would like to mention the colleagues from the EIC pfRICH collaboration and members of CFNS who provided tremendous help. This report is part of the pfRICH PED effort and is supported by funding from the JLab EIC project and the Center for Frontiers in Nuclear Science at Stony Brook.

A Surface Smoothness for different substrates

The amount of light reflected by a surface, and how it is reflected, is highly dependent upon the smoothness or texture of the surface. When surface imperfections are smaller than the wavelength of the incident light (as in the case of a mirror), virtually all of the light is reflected equally. However, in the real world, most objects have convoluted surfaces that exhibit a diffuse reflection, with the incident light being reflected in all directions. This interactive tutorial explores how light waves are reflected by smooth and rough surfaces.

The reflectivity could be broadly categorized into specular and diffuse reflection. The specular reflection is defined as light reflected from a smooth surface at a definite angle, and diffuse reflection, is produced by rough surfaces that tend to reflect light in all directions. There are far more occurrences of diffuse reflection than specular reflection in our everyday environment.

For the benefit of the Cherenkov detector performance, we desire the specular reflection as the direction/hit location of the photon on the detector follows the predictable optics principles (reflection and refraction). In this case, the requirement for the smoothness of the coated substrate is implied with a requirement of reflectivity specified.

Fig. 21 shows the visual quality for the coating substrate material of the CMA mirror sample, Lexan film with the protective coating and laminated carbon fiber sheet manufactured at Perdue University [3]. The smoothness of these substrate materials is measured by Perdue Composite Manufacturing & Simulation Center (CMSC). Sample data for the measurement is given in Tab. 5. The smoothness of the CMA sample mirror, Lexan 8010 with protective film and carbon fiber sheet is 0.01 μm, 0.17 μm, 0.3 μm, which corresponds to ISO N1, N2, and N4 polished finishes, respectively.

To achieve the requirement 300% reflectivity goal, the reflective substrate must have N1 (0.01μm) polished finish or better. Both the CMA sample and Lexan 8010 (without protective coating) sample satisfy such requirements [1]. Note that the product specification of Lexan 8010 is 0.01 μm.

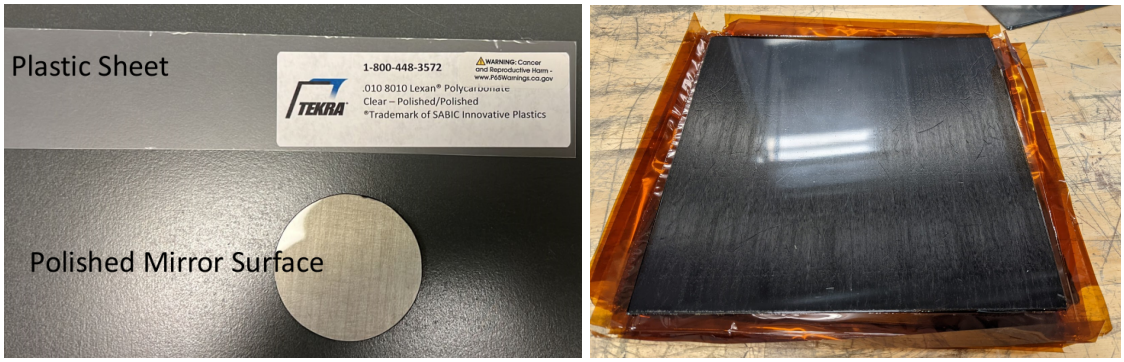

Figure 21: Left: showing the CMA mirror sample and Lexan 8010 plastic strip with a protective coating; Right: laminated carbon fiber backing produced at Purdue University.

Table 5: CMA (sample #14) Polished mirror surface data provided by A. Jung at Purdue University [2].

Test #	Ra (μm)	Rq (μm)	Rz(μm)
1	0.010	0.012	0.062
2	0.010	0.012	0.066
3	0.010	0.013	0.080
4	0.010	0.012	0.062
5	0.010	0.013	0.072
6	0.010	0.012	0.069
7	0.011	0.014	0.072
8	0.048	0.077	0.420
9	0.010	0.013	0.077
10	0.011	0.013	0.076
AVG	0.014	0.0191	0.1056

References

[1] Product manual: https://ff.sabic.eu/uploads/resources/1604271936-656637-LEXAN-8010-SHEETED-FILM-DATASHEET-2020.pdf.

[2] Internal presentation pfRICH meeting: https://indico.bnl.gov/event/20307.

[3] Email: anjung@purdue.edu.